Inorganic Chemistry
Article

Inorg. Chem. **2010**, *49*, 2093–2102 **2093**
DOI: 10.1021/ic9012119

A Star-Shaped Heteronuclear $Cr^{III}Mn^{II}_3$ Species and Its Precise Electronic and Magnetic Structure: Spin Frustration Studied by X-Ray Spectroscopic, Magnetic, and Theoretical Methods

Manuel Prinz,[†] Karsten Kuepper,[‡,♦] Christian Taubitz,[†] Michael Raekers,[†] Sumit Khanra,[§] Biplab Biswas,[§] Thomas Weyhermüller,[§] Marc Uhlarz,[∥] Joachim Wosnitza,[∥] Jürgen Schnack,[⊥] Andrei V. Postnikov,[#] Christian Schröder,[▽] Simon J. George,[○] Manfred Neumann,*[,†] and Phalguni Chaudhuri*[,§]

[†]*University of Osnabrück, Department of Physics, Barbarastrasse 7, D-49069 Osnabrück, Germany,* [‡]*Forschungszentrum Dresden-Rossendorf, Institut für Ionenstrahlphysik und Materialforschung, D-01314 Dresden, Germany,* [§]*Max-Planck-Institut für Bioanorganische Chemie, Stiftstrasse 34-36, D-45470 Mülheim an der Ruhr, Germany,* [∥]*Hochfeld-Magnetlabor Dresden, Forschungszentrum Dresden-Rossendorf, D-01314 Dresden, Germany,* [⊥]*Fakultät für Physik, Universität Bielefeld, Postfach 100131, D-33501 Bielefeld, Germany,* [#]*Laboratoire de Physique des Milieux Denses, Institut Jean Barriol, Paul Verlaine University, 1 Bd. Arago, 57078 Metz, France,* [▽]*University of Applied Sciences Bielefeld, Department of Engineering Sciences and Mathematics Wilhelm-Bertelsmann-Str. 10, D-33602 Bielefeld, Germany, and* [○]*Advanced Biological and Environmental X-ray Facility, Lawrence Berkeley National Laboratory, 1 Cyclotron Road, Berkeley, California 94720.* [♦] *Present address: University of Ulm, Department of Solid State Physics, Albert Einstein-Allee 11, 89069 Ulm, Germany.*

Received June 24, 2009

Molecular magnets incorporate transition-metal ions with organic groups providing a bridge to mediate magnetic exchange interactions between the ions. Among them are star-shaped molecules in which antiferromagnetic couplings between the central and peripheral atoms are predominantly present. Those configurations lead to an appreciable spin moment in the nonfrustrated ground state. In spite of its topologically simple magnetic structure, the $[Cr^{III}Mn^{II}_3(PyA)_6Cl_3]$ (**$CrMn_3$**) molecule, in which PyA represents the monoanion of *syn*-pyridine-2-aldoxime, exhibits nontrivial magnetic properties, which emerge from the combined action of single-ion anisotropy and frustration. In the present work, we elucidate the underlying electronic and magnetic properties of the heteronuclear, spin-frustrated **$CrMn_3$** molecule by applying X-ray magnetic circular dichroism (XMCD), as well as magnetization measurements in high magnetic fields, density functional theory, and ligand-field multiplet calculations. Quantum-model calculations based on a Heisenberg Hamiltonian augmented with local anisotropic terms enable us not only to improve the accuracy of the exchange interactions but also to determine the dominant local anisotropies. A discussion of the various spin Hamiltonian parameters not only leads to a validation of our element selective transition metal L edge XMCD spin moments at a magnetic field of 5 T and a temperature of 5 K but also allows us to monitor an interesting effect of anisotropy and frustration of the manganese and chromium ions.

1. Introduction

Magnetic materials comprising nanosized molecular building blocks have attracted large interest from several scientific disciplines. Chemically stable free radicals incorporated in purely organic compounds reveal long-range magnetic interactions at low temperatures. The flexibility available in carbon chemistry is exploited to synthesize such compounds. The most promising molecular magnets are polymetallic clusters, containing transition-metal ions bridged by molecular groups to mediate exchange interactions between the paramagnetic centers. Such interactions may result in ground states with a relatively large total spin (S).[1]

Compared to other transition metals, complexes containing manganese ions are especially often characterized by ground states with large magnetic moments, and this in

*To whom correspondence should be addressed. E-mail: chaudh@mpi-muelheim.mpg.de (P.C.), mneumann@uos.de (M.N.).

(1) (a) Blundell, S. J. *Contemp. Phys.* **2007**, *48*(5), 275–290. (b) Sessoli, R.; Gatteschi, D.; Caneschi, A.; Novak, M. *Nature* **1993**, *365*, 141–143. (c) Kahn, O. *Molecular Magnetism*; Wiley: Singapore, 1993.

Published on Web 01/28/2010

conjunction with the presence of highly Jahn−Teller distorted Mn ions makes manganese clusters ideal candidates for high-spin molecules.[2] Due to the combined action of intramolecular exchange and large negative (easy-axis-type) magnetoanisotropy (D), the phenomenon of single-molecule magnetism (SMM) arises for such compounds, for which a significant barrier to thermally activated magnetization relaxation is characteristic.[3]

Very intensively investigated molecular magnets are the dodecanuclear complexes $[Mn_{12}O_{12}(O_2CR)_{16}(H_2O)_x]^{n-}$ (n = 0, 1, 2; x = 3, 4), but also manganese-containing polymetallic clusters with nuclearity ranging from 2 to 84 have been synthesized and reveal a large spin ground state and magnetoanisotropy.[4] The up to date highest blocking temperature is reached in hexanuclear manganese compounds.[5,6] Because these molecules display not only a magnetization hysteresis but also quantum tunneling of magnetization (QTM)[7,8] and quantum interference,[9] they are promising new materials for practical applications like ultradense magnetic data storage, quantum computing, or other interesting devices.[10−12] These properties are governed by the already mentioned magnetic anisotropy barrier of the magnetic core, which originates from the spin−orbit coupling in the paramagnetic ions in a high-spin state.[13] For a better understanding especially of the microscopic mechanisms, experimental and theoretical investigations in high-spin molecules are required.

Regarding the interplay of topology and exchange interactions in polynuclear high-spin clusters, another interesting effect can be observed: magnetic frustration which appears due to, e.g., triangular arrangements of antiferromagnetic exchange pathways.[14] Geometric frustration of interacting spins leads to a variety of fascinating phenomena[14−16] in low-dimensional and molecular magnetism: (1) a nontrivially, i.e., orbitally, degenerate ground state;[17,18] (2) many low-lying nonmagnetic excitations below the first triplet excitation;[19] (3) magnetization plateaus of the magnetization curve $M(B)$ at T = 0;[24] (4) large magnetization jumps at T = 0;[24] (5) (quantum) phase transitions at T = 0.[16] These phenomena do not occur in so-called bipartite spin systems, i.e., spin systems that can be divided into two sublattices.[20−22] Very prominent examples of geometrically frustrated spin systems exhibiting a rich spectrum of frustration phenomena are the giant Keplerate molecules.[23−25]

The present publication is devoted to the study of the electronic and revisited magnetic properties of an amazing manganese-containing high-spin molecule: the spin-frustrated star-shaped heterotetranuclear $Cr^{III}Mn^{II}_3$ complex.[26] The investigations of topologically similar, but chemically different, ferric and manganese star-shaped molecules show that there are star-shaped molecules in which predominately antiferromagnetic couplings of the central ion with its peripheral neighbors lead to an appreciable spin moment in the nonfrustrated ground state.[27−29] In spite of its topologically simple magnetic system, the $[Cr^{III}Mn^{II}_3(PyA)_6Cl_3]$ molecule (**$CrMn_3$**) exhibits the above-mentioned nontrivial magnetic properties, *single-ion anisotropy and frustration*, bearing interesting consequences for the chromium ion.

The tetranuclear complex contains three Mn^{2+} ions ($3d^5$, high-spin, S = 5/2) and a single Cr^{3+} ion ($3d^3$, high-spin, S = 3/2). The expected saturation magnetization is actually reached at a magnetic field of about 12 T at 1.8 K. The special form of the magnetization curve gives rise to the assumption that anisotropy and frustration effects are of great importance.

Here, we show that X-ray magnetic circular dichroism (XMCD) is a very powerful technique to study heteronuclear molecule-based magnets because of its generally high sensitivity to the local electronic structure, and moreover by the force of element and shell selectivity of the Mn^{2+} and Cr^{3+} ions in our case. Furthermore, XMCD is one of the rare experimental methods to determine element-selective

(2) Hendrickson, D. N.; Christou, G.; Ishimoto, H.; Yoo, J.; Brechin, E. K.; Yamaguchi, A.; Rumberger, E. M.; Aubin, S. M. J.; Sun, Z.; Aromi, G. *Mol. Cryst. Liq. Cryst.* **2002**, *376*, 301–313.
(3) Sessoli, R.; Gatteschi, D.; Hendrickson, D. N.; Christou, G. *MRS Bull.* **2000**, *25*, 66–71.
(4) See, for example: (a) Tasiopoulos, A. J.; Vinslava, A.; Wernsdorfer, W.; Abboud, K. A.; Christou, G. *Angew. Chem., Int. Ed.* **2004**, *43*, 2117–2121. (b) Miyasaka, H.; Clérac, R.; Wernsdorfer, W.; Lecren, L.; Bonhomme, C.; Sugiura, K.; Yamashita, M. *Angew. Chem., Int. Ed.* **2004**, *43*, 2801–2805. (c) Murugesu, M.; Wernsdorfer, W.; Raftery, J.; Christou, G.; Brechin, E. K. *Inorg. Chem.* **2004**, *43*, 4203–4209. (d) Milios, C. J.; Raptopoulou, C. P.; Terzis, A.; Lloret, F.; Vicente, R.; Perlepes, S. P.; Escuer, A. *Angew. Chem., Int. Ed.* **2003**, *43*, 210–212. (e) Wittick, L. M.; Murray, K. S.; Moubaraki, B.; Batten, S. R.; Spiccia, L.; Berry, K. J. *Dalton Trans.* **2004**, 1003–1011.
(5) Milios, C. J.; Vinslava, A.; Wernsdorfer, W.; Moggach, S.; Parsons, S.; Perlepes, S. P.; Christou, G.; Brechin, E. K. *J. Am. Chem. Soc.* **2007**, *129*, 2754.
(6) Carretta, S.; Guidi, T.; Santini, P.; Amoretti, G.; Pieper, O.; Lake, B.; van Slageren, J.; El Hallak, F.; Wernsdorfer, W.; Mutka, H.; Russina, M.; Milios, C. J.; Brechin, E. K. *Phys. Rev. Lett.* **2008**, *100*, 157203.
(7) Friedman, J. R.; Sarachik, M. P.; Tejada, J.; Ziolo, R. *Phys. Rev. Lett.* **1996**, *76*, 3830–3833.
(8) Thomas, L.; Lionti, F.; Ballou, R.; Gatteschi, D.; Sessoli, R.; Barbara, B. *Nature* (*London*) **1996**, *383*, 145.
(9) Wernsdorfer, W.; Sessoli, R. *Nature* **1999**, *284*(5411), 133–135.
(10) Verdaguer, M.; Bleuzen, A.; Train, C.; Garde, R.; Fabrizi de Biani, F.; Desplanches, C. *Philos. Trans. R. Soc. A* (*London*) **1999**, *357*, 2959.
(11) Leuenberger, M. N.; Loss, D. *Nature* (*London*) **2001**, *410*, 789.
(12) Ohkoshi, S.-I.; Hashimoto, K. *Electrochem. Soc. Interface* **2002**, *11*, 34.
(13) van Vleck, J. *Phys. Rev.* **1937**, *52*, 1178.
(14) Greedan, J. *J. Mater. Chem.* **2001**, *11*, 37.
(15) Schnack, J Molecular Magnetism. In *Lecture Notes in Physics 645*; Springer: Berlin, 2004; pp 155−194.
(16) Schröder, C.; Schmidt, H.-J.; Schnack, J.; Luban, M. *Phys. Rev. Lett.* **2005**, *94*, 207203.
(17) Dai, D; Whangbo, M.-H. *J. Chem. Phys.* **2004**, *121*(2), 672.
(18) Kahn, O. *Chem. Phys. Lett.* **1997**, *265*, 109–114.
(19) (a) Schmidt, R.; Richter, J.; Schnack, J. *J. Magn. Magn. Mater.* **2005**, *295*(2), 164–167. (b) Waldtmann, C.; Everts, H. U.; Bernu, B.; Lhuillier, C.; Sindzingre, P.; Lecheminant, P.; Pierre, L. *Eur. Phys. J. B* **1998**, *2*, 501. (c) Moessner, R. *Can. J. Phys.* **2001**, *79*, 128.
(20) Lieb, E. H.; Schultz, D. T.; Mattis, D. C. *Ann. Phys.* (*N.Y.*) **1961**, *16*, 407.
(21) Lieb, E. H.; Mattis, D. C. *J. Math. Phys.* **1962**, *3*, 749.
(22) Schnack, J. *J. Low Temp. Phys.* **2006**, *142*(3−4), 279–284.
(23) Müller, A. *Chem. Phys. Chem.* **2001**, *2*, 517.
(24) (a) Schröder, C.; Nojiri, H.; Schnack, J.; Hage, P.; Luban, M.; Kögerler, P. *Phys. Rev. Lett.* **2005**, *94*, 017205. (b) Rousochatzakis, I.; Läuchli, A. M.; Mila, F. *Phys. Rev. B* **2008**, *77*, 094420. (c) Schulenburg, J.; Honecker, A.; Schnack, J.; Richter, J.; Schmidt, H.-J. *Phys. Rev. Lett.* **2002**, *88*, 167207.
(25) Schröder, C.; Prozorov, R.; Kögerler, P.; Vannette, M. D.; Fang, X.; Luban, M.; Matsuo, A.; Kindo, K.; Müller, A.; Todea, A. M. *Phys. Rev. B* **2008**, *77*, 224409.
(26) Khanra, S.; Biswas, B.; Golze, C.; Büchner, B.; Kataev, V.; Weyhermüller, T.; Chaudhuri, P. *Dalton Trans.* **2007**, 481–487.
(27) Saalfrank, R. W.; Scheurer, A.; Bernt, I.; Heinemann, F. W.; Postnikov, A. V.; Schünemann, V.; Trautwein, A. X.; Alam, M.; Rupp, H.; Müller, P. *Dalton Trans.* **2006**, *23*, 2865.
(28) Takács, A. F.; Neumann, M.; Postnikov, A. V.; Kuepper, K.; Scheurer, A.; Sperner, S.; Saalfrank, R. W.; Prince, K. C. *J. Chem. Phys.* **2006**, *124*, 4503.
(29) (a) Khanra, S.; Kuepper, K.; Weyhermüller, T.; Prinz, M.; Raekers, M.; Voget, S.; Postnikov, A. V.; de Groot, F. M. F.; George, S. J.; Coldea, M.; Neumann, M.; Chaudhuri, P. *Inorg. Chem.* **2008**, *47*. (b) Arroi, M.-A.; Sculiller, A.; Cartier dit Moulin, Ch.; Sainctavit, Ph.; Mallah, T.; Verdaguer, M. *J. Am. Chem. Soc.* **1999**, *121*, 6414.

spin and orbital moments separately in heteronuclear systems.[30,31]

This article is arranged as follows. In section 2, we give a brief overview of the molecular structure and basic magnetic properties. Later on, the experimental and theoretical procedures are described in section 3. We present a detailed analysis of the advanced magnetic properties by means of magnetization measurements using a high-magnetic-field extraction technique (up to $B = 14$ T). On the basis of the high-field measurements, theoretical simulations using an anisotropic spin Hamiltonian are presented. These simulations enable us not only to supply accurate values of the exchange interactions but also to determine the dominant local anisotropies. A discussion of the various spin-Hamiltonian parameters leads to a validation of our element-selective transition-metal L-edge XMCD spin-moment contribution presented in section 4. Here, we also provide charge-transfer multiplet model calculations for the chromium L edge to discuss the valence and crystal-field excitations, along with the results of calculations, within the density functional theory, of spatial spin density. Finally, we end up with our main conclusions in section 5.

2. Structure and Magnetic Properties of $[Cr^{III}Mn^{II}_3(PyA)_6Cl_3]$

The synthesis and structure refinement of the present heterotetranuclear complex have been carried out at the Max-Planck-Institute for Bioinorganic Chemistry at Mülheim a. d. Ruhr, Germany. Khanra et al. reported earlier magnetic and HF-EPR measurements of this spin-frustrated compound.[26] The tetranuclear star-shaped complex $[Cr^{III}Mn^{II}_3(PyA)_6Cl_3]$ (**$CrMn_3$**) molecule contains a $Cr^{III}Mn^{II}_3$ trigonal core with a Cr(1) atom surrounded by three Mn(1) centers at the apexes of an equilateral triangle (Figure 1), so that the cluster comprises the C_3 symmetry. The three Mn(II) ions form an equilateral triangle with the Cr(III) ion placed above the Mn−Mn−Mn plane (chlorine atoms below). The peripheral manganese centers, 6-fold coordinated in highly distorted $MnOClN_4$ cores, are linked through the oximate (μ_2-O−N) group. Each Mn(II) ion is linked to the central Cr(1) atom through two oximate (N−O) and one μ_2-O_{ox} donor. The central chromium atom Cr(1) is in almost perfect octahedral coordination. The six oximato oxygen ligands (deviation from 90° being less than 1.8°), O(1), and O(11) and their equivalents are pendant from the three peripheral $Mn(PyA)_2$ fragments. It was concluded that the **$CrMn_3$** complex contains a $Cr^{III}Mn^{II}_3$ (high spin) core.[26]

The magnetization of a polycrystalline **$CrMn_3$** sample has been measured between 2 and 290 K in magnetic fields of 1, 4, and 7 T. EPR spectra have been collected at a temperature of 10 K in magnetic fields up to 15 T and in a frequency range between 19 and 388 GHz. The investigations revealed the following conclusions:

The exchange interactions $J_{CrMn} = -0.29$ cm^{-1} and $J_{MnMn} = -0.07$ cm^{-1}, defined by eq 1 and shown as

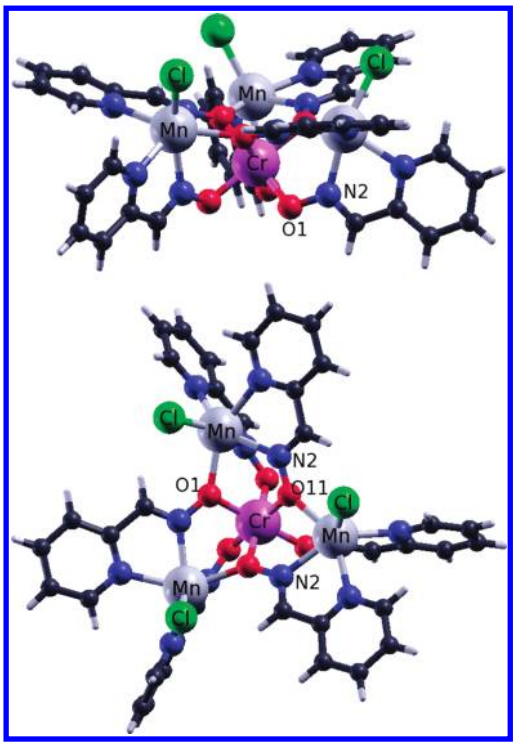

Figure 1. Two perspective views of the $[Cr^{III}Mn^{II}_3(PyA)_6Cl_3]$ molecule. The labeling O1, O11, and N2 is after ref 26. The figure was created with the XCrySDen software.[57]

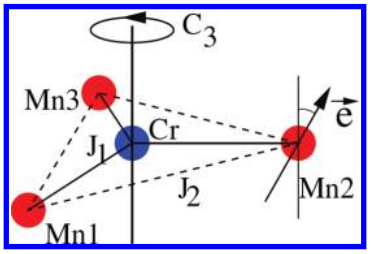

Figure 2. Schematic structure of the **$CrMn_3$** molecule. The central chromium spin is antiferromagnetically coupled by $J_1 = J_{Cr-Mn}$ to the three surrounding manganese ions (solid lines). The manganese ions are coupled antiferromagnetically with each other by the exchange interaction $J_2 = J_{Mn-Mn}$ (dashed lines). The dominant local anisotropy axes are given by the unit vectors $\vec{e}_k$.

J_1 and J_2 in Figure 2, are weakly antiferromagnetic. This is not common among Cr(III) and Mn(II) ions in triply oximato-bridged complexes.[32]

The experimental magnetization data could not be simulated without taking into account exchange interactions between the Mn(II) spins connected through an oximate bridge, although the peripheral Mn···Mn distances are long at 5.49 Å. A zero-field spitting parameter D of -1 cm^{-1} was found from the magnetic measurements in agreement with the HF-EPR measurements.[26] For a more detailed structural and magnetochemical characterization, see ref 26.

(30) Chen, C. T.; Idzerda, Y. U.; Lin, H.-J.; Smith, N. V.; Meigs, G.; Chaban, E.; Ho, G. H.; Pellegrin, E.; Sette, F. *Phys. Rev. Lett.* **1995**, *75*, 152–155.

(31) Funk, T.; Deb, A.; George, S. J.; Wang, H. X.; Cramer, S. P. *Coord. Chem. Rev.* **2005**, *249*, 3.

(32) (a) Ross, S.; Weyhermüller, T.; Bill, E.; Wieghardt, K.; Chaudhuri, P. *Inorg. Chem.* **2001**, *40*, 6656. (b) Ross, S.; Weyhermüller, T.; Bill, E.; Bothe, E.; Flörke, U.; Wieghardt, K.; Chaudhuri, P. *Eur. J. Inorg. Chem.* **2004**, 984. (c) Weyhermüller, T.; Wagner, R.; Khanra, S.; Chaudhuri, P. *Dalton Trans.* **2003**, 2539. (d) Khanra, S.; Weyhermüller, T.; Rentschler, E.; Chaudhuri, P. *Inorg. Chem.* **2005**, *44*, 8176.

3. Experimental and Theoretical Procedures

3.1. Experimental Methods. 3.1.1. X-Ray Spectroscopic Techniques. The XMCD spectroscopy was performed at the elliptically polarizing undulator beamline 4.0.2 of the Advanced Light Source (ALS), Berkeley, California.[33] The samples were mounted into a cryostat equipped with a 6-T superconducting magnet;[34] the sample stage was connected to a pumped helium cryostat reaching base temperatures of around 20.0 and 5.0 K during the experiments presented here. The measurements at the Mn L edge have been recorded under external magnetic fields of different strengths in the total electron yield (TEY) mode.

3.1.2. Magnetization Measurements. The magnetization measurements were performed in a commercial PPMS magnetometer (Quantum Design, 6325 Lusk Boulevard, San Diego, CA 92121-3733) equipped with a superconducting 14-T magnet. The magnetic moment of the samples was determined by use of a DC extraction-mode technique after careful temperature and field stabilization. For each measurement, the sample was moved at a high, uniform speed through a detection coil set. The sample moment was then derived from the recorded profile of induction voltage versus sample position. Each measurement at fixed temperature and magnetic field was performed five times in rapid succession, in order to obtain an averaged value for better resolution.

3.2. Theory. 3.2.1. Density-Functional Theory. The electronic structure was calculated by use of the generalized gradient approximation of the density functional theory,[35,36] using the SIESTA (Spanish Initiative for Electronic Simulations with Thousands of Atoms) calculation method.[37,38] More details and results will be published elsewhere along with X-ray electron and emission spectroscopic data.[39]

3.2.2. Ligand-Field Multiplet Model. The XAS lineshapes of the chromium $L_{2,3}$ edge were simulated within charge transfer multiplet-model calculations (CTM) using the TTmultiplet program.[40] First, the energy levels of the initial state ($2p^63d^3$) and final state ($2p^53d^4$) were calculated in spherical (O_3) symmetry. The parameters include the spin−orbit coupling of the 2p core and 3d valence-band electrons, the 3d3d as well as the 2p3d Slater integrals in the initial and final states. The d−d and p−d integrals were reduced to 80% of their atomic Hartree−Fock values, whereas the spin−orbit parameters were not reduced. Then, a cubic crystal field (O_h symmetry) of 10 Dq = 2.2 eV strength was considered in the crystal-field approach. Finally, a charge transfer configuration $3d^4\underline{L}$ was considerd. The energy difference between the two configurations $E(2p^63d^3) - E(2p^63d^4\underline{L}) = \Delta$ was set to 4.0 eV. For comparison with experimental results, the lifetime broadening of the 2p core hole and the resolution of the spectrometer were taken properly into account.

3.2.3. Simulations with Anisotropic Spin Hamiltonians. In order to model the spin system of **$CrMn_3$**, the following microscopic spin Hamiltonian has been used[6,41,42]

$$H = -2\sum_{k<l} J_{kl}\vec{s}_k\cdot\vec{s}_l + \sum_k d_k(\vec{e}_k\cdot\vec{s}_k)^2 + \mu_B\sum_k \vec{B}\cdot g_k\cdot\vec{s}_k \quad (1)$$

The first term accounts for the superexchange coupling between the paramagnetic centers (Heisenberg term). For **$CrMn_3$**, we employ two couplings: J_{Cr-Mn} for the interaction of the central chromium spin with the three surrounding manganese ions (solid lines in Figure 2) and J_{Mn-Mn} for the interaction between the manganese ions (dashed lines in Figure 2).

The second term in eq 1 models the single-ion anisotropy of Mn and Cr, respectively, by means of the dominant axis of the local anisotropy tensor (so-called D term). The unit vectors $\vec{e}_k$ set the directions of the local anisotropy axes. The prefactors d_k denote the strength of the local anisotropy; a negative value corresponds to an easy axis, a positive one to a hard axis. The last term in eq 1 reflects the interaction with the applied magnetic field (Zeeman term). In this work, we assume an isotropic **g** tensor. Since we investigated a powder sample, an orientational average is applied using discrete Lebedev−Laikov grids.[43]

We have also performed classical spin-dynamic simulations in order to investigate the field-dependent classical ground state and low-temperature properties, in particular to study the role of the exchange couplings and anisotropies for certain temperatures and external magnetic fields. We write the Hamiltonian of the classical system as

$$H_c = -2\sum_{k<l} J^c_{kl}\vec{m}_k\cdot\vec{m}_l + \sum_k d^c_k(\vec{e}_k\cdot\vec{m}_k)^2 + \mu_c\sum_k \vec{B}\cdot\vec{m}_k \quad (2)$$

The spins $\vec{m}_k$ are classical unit vectors whose orientations are specified by the polar and azimuthal angles, θ_i and φ_i, all extending from 0 to π and 0 to 2π, respectively. The Hamiltonian of eq 2 provides the classical counterpart to the quantum Heisenberg model eq 1. This correspondence is achieved by replacing in eq 1 all quantum spin operators by $\vec{s}_k = \sqrt{s_k(s_k+1)}\cdot\vec{m}_k$, with s_k describing the spin quantum number of a given ion.[44] It thus follows that $J^c_{kl} = \sqrt{s_k(s_k+1)s_l(s_l+1)}\cdot J_{kl}$ and $d^c_k = s_k(s_k+1)d_k$; moreover, the quantity μ_c in eq 1 is given by $\mu_c = (g_k\mu_B)\sqrt{s_k(s_k+1)}$ where g_k is the Landé g factor for a given ion and μ_B is the Bohr magneton. We have checked the applicability of our classical treatment by comparing the results of classical Monte Carlo calculations with the above-described exact quantum model calculations.

Furthermore, we have studied the low-temperature field-dependent spin dynamics. An effective method for investigating this property is to use the numerical solution of the stochastic Landau−Lifshitz equation which simulates the time evolution of the spin system coupled to the heat bath. Fluctuating fields with white noise characteristics are used to account for the effects of the interaction of the spin system with the heat bath. Those environmental degrees of freedom are also responsible for the damped precession of the magnetization parametrized by a phenomenological damping factor.

(33) Young, A. T.; Martynov, V.; Padmore, H. A. *J. Electron. Spectrosc. Relat. Phenom.* **1999**, *103*, 885.
(34) Funk, T.; Friedrich, S.; Young, A.; Arenholz, E.; Cramer, S. P. *Rev. Sci. Instrum.* **2002**, *73*, 1649.
(35) Perdew, J. P.; Burke, K.; Ernzerhof, M. *Phys. Rev. Lett.* **1996**, *77*(18), 3865–3868.
(36) Perdew, J. P.; Burke, K.; Ernzerhof, M. *Phys. Rev. Lett.* **1997**, *78*(7), 1396.
(37) Soler, J. M.; Artacho, E.; Gale, J. D.; García, A.; Junquera, J.; Ordejón, P.; Sánchez-Portal, D. *J. Phys.: Condens. Matter* **2002**, *14*(11), 2745–2779.
(38) Siesta - Home. http://www.uam.es/siesta (accessed Jan 2010).
(39) Postnikov, A. V. Manuscript in preparation.
(40) (a) de Groot, F. M. F. *J. Electron. Spectrosc. Relat. Phenom.* **1994**, *67*, 529. (b) de Groot, F. M. F. *Coord. Chem. Rev.* **2005**, *249*, 31. (c) Butler, P. H. *Point Group Symmetry, Applications, Methods and Tables*; Plenum: New York, 1981. (d) Cowan, R. D. *The Theory of Atomic Structure and Spectra*; University of California Press: Berkeley, 1981.
(41) Schnack, J.; Brüger, M.; Luban, M.; Kögerler, P.; Morosan, E.; Fuchs, R.; Modler, R.; Nojiri, H.; Rai, R. C.; Cao, J.; Musfeldt, J. L.; Wei, X. *Phys. Rev. B* **2006**, *73*, 094401.
(42) (a) Glaser, T.; Heidemeier, M.; Krickemeyer, E.; Bögge, H.; Stammler, A.; Fröhlich, R.; Bill, E.; Schnack, J. *Inorg. Chem.* **2009**, *48*(2), 607–620. (b) Schnack, J. *Magn. Condens. Matter Phys.* **2009**, *12*, 323–330.
(43) Lebedev, V. I.; Laikov, D. N. *Dokl. Math.* **1999**, *59*(3), 477–481.
(44) Ciftja, O.; Luban, M.; Auslender, M.; Luscombe, J. H. *Phys. Rev. B* **1999**, *60*, 10122.

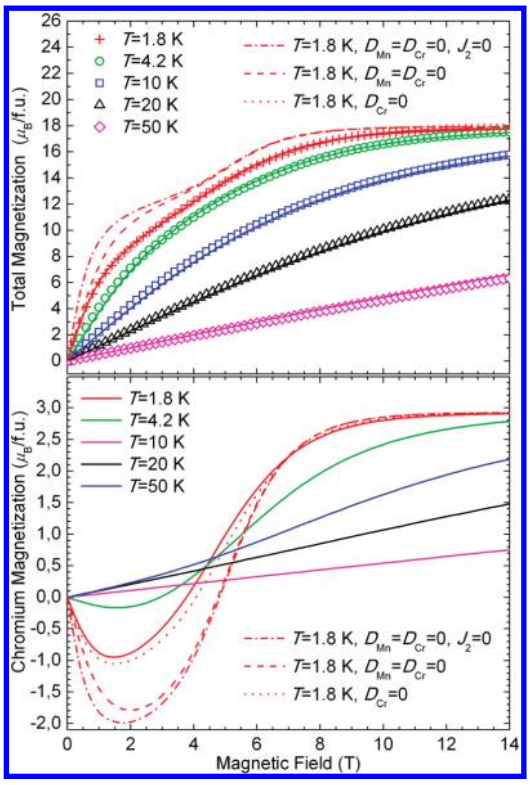

Figure 3. Top panel: Magnetic-field dependence of the magnetization per $[Cr^{III}Mn^{II}_3(PyA)_6Cl_3]$ molecule. The experimental data for various temperatures are given by symbols. The lines represent theoretical estimates using the parameters given in the text. Bottom panel: Theoretical estimates of the local magnetization of the center Cr ion in the **$CrMn_3$** magnetic core for various temperatures. See text for more details.

4. Results and Discussion

4.1. Magnetization Measurements and Anisotropic Spin-Hamiltonian Simulations. Some gross properties of the magnetic heterotetranuclear complex $[Cr^{III}Mn^{II}_3(PyA)_6Cl_3]$ have been investigated previously. It has been found that, besides a dominant antiferromagnetic exchange interaction between the central chromium spin ($s_{Cr} = 3/2$) and its surrounding manganese spins ($s_{Mn} = 5/2$), a frustrating antiferromagnetic coupling between the manganese ions exists.[26] A sizable zero-field splitting was also inferred from EPR measurements. In this section, we report on detailed investigations of the microscopic parameters of **$CrMn_3$**.

For a more detailed study of the magnetic properties of **$CrMn_3$**, the magnetization of a polycrystalline sample has been measured at high magnetic fields by using a standard inductive method. Magnetic fields from 0 to 14 T at temperatures of 1.8, 4.2, 10, 20, and 50 K have been applied. The results are shown by symbols in the upper panel of Figure 3. The observed magnetic-field dependence of the magnetization as well as the field needed to reach saturation at 18 μ_B ($s_{Cr} = 3/2, 3s_{Mn} = 5/2$) reflects a nontrivial magnetic interaction between the magnetic ions. Near $B = 0$, a detailed analysis revealed no magnetic hysteresis.

The high-field magnetization measurements enable us not only to determine accurately the exchange interactions but also to determine the dominant local anisotropies. To this end, Hamiltonian 1 is used. Following ref 26, we assume that **$CrMn_3$** possesses C_3 symmetry; i.e., the exchange coupling J_{Cr-Mn} of the central chromium is the same for all three surrounding manganese ions, and J_{Mn-Mn} is equal between the latter. For the local anisotropies, this symmetry implies that the anisotropy axes of the manganese ions share a common angle ϑ with respect to the C_3 axis of the molecule. The azimuthal angles ϕ_κ differ by 120° between adjacent spins. Their exact orientation relative to the molecular skeleton cannot be specified since neither the two other principal axes of the **d** tensor (so-called E-terms) nor the coupling of spins to orbital/structural parameters have been included in the spin-Hamiltonian. For chromium, the C_3 symmetry implies that its anisotropy axis coincides with the rotational one of the molecule. Using these assumptions, we arrive at a fit describing best the magnetization data shown in Figure 3 (top panel) for $J_{Cr-Mn} = -0.29\ cm^{-1}$, $J_{Mn-Mn} = -0.07\ cm^{-1}$, $d_{Mn} = -1.05\ cm^{-1}$, $\vartheta_{Mn} = 15°$, and $d_{Cr} = 0.40\ cm^{-1}$. We used $g_{Mn} = 2.0$ and $g_{Cr} = 1.95$ as in ref 26. The exchange couplings differ somewhat from those found in ref 26, since we now have incorporated the local anisotropies in the spin Hamiltonian, eq 1. On first glance, it is astonishing that Mn(II) with a half-filled d shell should have an anisotropy as large as $d_{Mn} = -1.05\ cm^{-1}$. However, the 6-fold coordination of the manganese ions in **$CrMn_3$** results in a highly distorted $MnOClN_4$ core. In such a distorted local environment, Mn(II) can reach anisotropies of up to 1.5 cm^{-1}, as has been shown in recent investigations.[45,46] Concerning ϑ_{Mn}, we would like to mention that there are Mn−Cl bonds pointing out of the Mn_3 plane, and it is well conceivable that the directions of the Mn anisotropy axes are fixed by the Cl ions. The accuracy of the fit depends differently on the various parameters. Variations of the exchange parameters as well as of the manganese anisotropy strength have drastic consequences, whereas variations of ϑ_{Mn} and of the chromium anisotropy do influence the fit only mildly. We assumed isotropic **g** tensors for simplicity. An inclusion of an improved **g** tensor, reasonably deviating from 2.0, might modify the obtained values, but not much.

The theoretical results with the above parameters (solid lines) are compared to the experimental data (symbols) in the upper panel of Figure 3. We would like to discuss the influence of the various spin-Hamiltonian parameters on the magnetization. To this end, we show for $T = 1.8$ K, as a dashed-dotted curve, the result corresponding to the case where only the coupling between the manganese and chromium ions is considered, and all other terms are set to zero. Such a system would be bipartite, i.e., nonfrustrated. An inclusion of the manganese−manganese coupling results in a weak frustration. The result is depicted by the dashed curve; the deviation from the bipartite system is largest at low fields. The dotted curve, which is hardly visible on top of the solid line, presents the result for the case of manganese anisotropies included as well. The chromium anisotropy then contributes only a minor improvement to the final fit.

(45) Duboc, C.; Collomb, M. N.; Pécaut, J.; Deronzier, A.; Neese, F. *Chem.—Eur. J.* **2008**, *14*, 6498–6509.
(46) Pichon, C.; Mialane, P; Rivière, E.; Blain, G.; Dolbecq, A.; Marrot, J.; Sécheresse, F.; Duboc, C. *Inorg. Chem.* **2007**, *46*, 7710–7712.

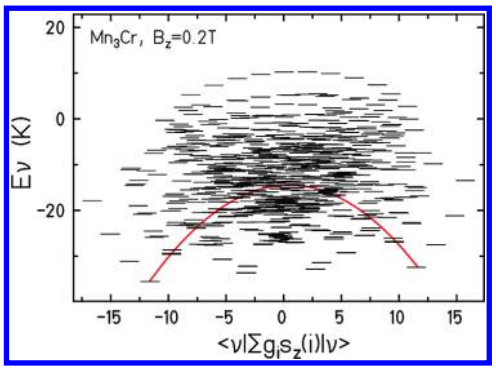

Figure 4. Energy spectrum of the $\mathbf{CrMn_3}$ magnetic core evaluated at a magnetic field of $B_z = 0.2$ T to separate degenerate states. The solid line shows a fictitious anisotropy barrier derived from the two lowest-energy eigenvalues on either side. The corresponding zero-field splitting parameter of these curves is $D = -0.575$ K.

Referring to the lower panel of Figure 3, we discuss the theoretical behavior of the chromium moment as a function of field for the same temperatures as in the top panel. At a low temperature ($T = 1.8$ K) and fields below 3 T, the chromium moment points predominantly opposite of the field direction. This can be understood from the fact that the three dominating manganese moments align themselves along the field direction, whereas the Cr moment, that is antiferromagnetically coupled to each of latter, points in the opposite direction. Thus, the Cr moment is largely reduced by frustration and anisotropy. For $T = 1.8$ K, indeed, the bipartite case (only $J_{\mathrm{Cr-Mn}} \neq 0$) shows the largest antiparallel alignment. The frustration due to $J_{\mathrm{Mn-Mn}}$ reduces the Cr moment somewhat. The largest impact arises from the manganese anisotropy, which reduces the chromium moment at $B = 2$ T by about a factor of 2. Counterintuitively, the chromium anisotropy has little influence on the chromium moment (dotted curve). Due to the given functional dependence of the chromium moment, its expectation value virtually vanishes in certain temperature and field regions, i.e., around 5 K and in fields of up to about 4.

To discuss the uniaxial anisotropy, we refer to Figure 4, which shows the energy eigenvalue spectrum of the $\mathbf{CrMn_3}$ magnetic core. Since the Hamiltonian is anisotropic, these eigenvalues do not belong to multiplets of the total spin. Nevertheless, they can be correlated with the total magnetization of the respective eigenstate, which depends on field. In order to split possible degeneracies, we present the eigenvalues at a rather small field of $B_z = 0.2$ T along the molecular C_3 axis. As can be derived from the data and qualitatively seen in the figure, the total ground state at $B = 0$ is 2-fold degenerate with a magnetization of approximately $\pm 12\ \mu_B$.

One can also see that these states do not belong to a well-separated ground-state multiplet, which is only split by anisotropy terms. On the contrary, the spectrum is rather dense. If one would try to attach an anisotropy barrier to the two ground states ($M \approx \pm 6$) and the next higher-lying states with $M \approx \pm 5$, one would arrive at an anisotropy barrier as given by the solid line in Figure 5. The corresponding zero-field splitting parameter is $D = -0.575$ K. Nevertheless, this discussion is purely fictitious. What would be needed to constitute a single molecule magnet is that the local Mn anisotropy axes would be aligned parallelly.

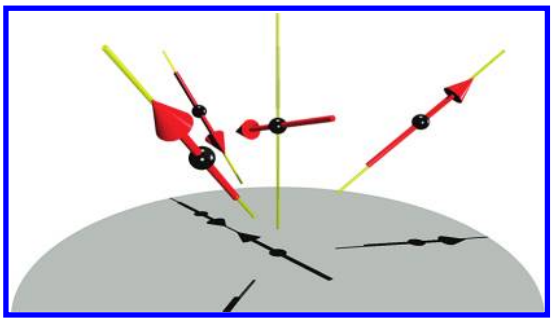

Figure 5. Classical ground-state configuration of $\mathbf{CrMn_3}$ as obtained by spin dynamics simulations at $T = 0$ and $B = 0$.

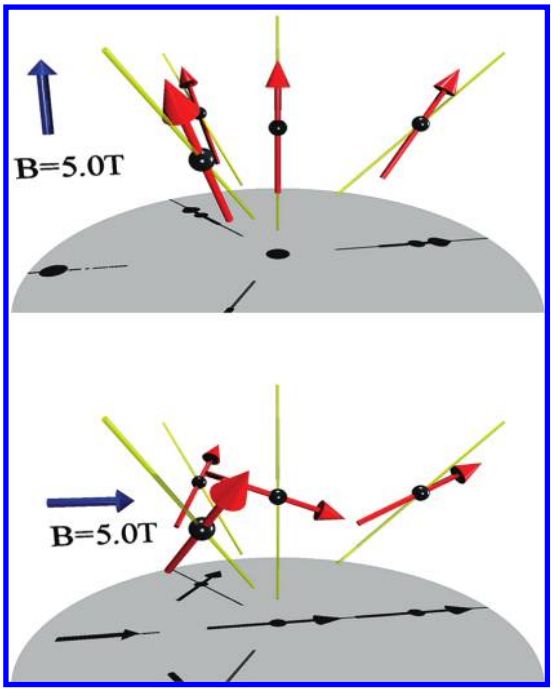

Figure 6. Classical ground-state configuration of $\mathbf{CrMn_3}$ as obtained by spin-dynamic simulations at $T = 0$ and an external field $B = 5$ T applied in different directions.

In Figure 5, we show the classical ground-state configuration of $\mathbf{CrMn_3}$ as obtained by classical spin-dynamics simulations at $T = 0$ and $B = 0$. The local anisotropy axes are depicted as yellow sticks. According to the model parameters, the strong easy-axis anisotropy dominates the orientation of the manganese spins in an up−up−down fashion, almost independent of the rather weak exchange interactions in the system. Only a very small canting with respect to the anisotropy axes is visible. The easy-plane anisotropy of the central chromium spin becomes apparent, with a small canting in the direction of the downward pointing manganese spin. This situation changes when an external field is applied. In Figure 6, we show simulation results for the spin orientations in an external field of 5 T applied along two different directions. Compared to the ground state at 0 T, one manganese spin is flipped, so that the up−up−down configuration is replaced by an up−up−up configuration in both cases. At 5 T, the Zeeman energy is much larger than the exchange interactions between all spins. However, the system is not yet fully saturated due to the fact that the anisotropy is still important.

We performed as well finite-temperature Monte Carlo and spin-dynamic simulations. For temperatures not too low ($T \approx 5$ K), our classical Monte Carlo simulations show qualitatively the same results as the "exact" quantum calculations. In particular, the element-specific magnetization curves show a vanishing local moment at the central chromium site at around 5 T. By using our stochastic Landau−Lifshitz method, we can directly study the time evolution of the classical spin system coupled to a heat bath at this field value. Here, we find a rather large and "stiff" local magnetic moment at the manganese sites; i.e., thermal fluctuations have little influence on the spin-vector motion due to the large local anisotropies. In contrast to this, the central chromium spin-vector motion is heavily influenced by thermal fluctuations.[47] We have found that its net moment is only nonzero for the component in the external field direction. Therefore, an orientational average would lead to a vanishing moment as derived from our magnetization data and as observed in our XMCD measurements (see below).

4.2. X-Ray Magnetic Circular Dichroism. In this section, we report on our detailed study of the XMCD transition-metal $L_{2,3}$ spectra of the paramagnetic centers, manganese and chromium, in the **$CrMn_3$** complex. The Cr XAS spectrum of **$CrMn_3$** is compared to ligand-field multiplet model calculations, whereas the Mn XMCD spectra are matched to the spectra and corresponding CTM calculations of our earlier investigations of a star-shaped $S_t = 10$ high-spin molecule with a $Mn^{II}{}_4O_6$ core (MnStar).[29] For this polymetallic complex with very weak exchange coupling, it was possible to probe almost the complete magnetic moment at the manganese ions by XMCD, yielding a giant total magnetic moment of 20 μ_B per molecule.

The **$CrMn_3$** and MnStar Mn $L_{2,3}$ X-ray absorption spectra excited by soft X-rays with 90% left and right circularly polarized light measured at 5 T and 5 K are presented in the top panel of Figure 7. The bottom panel displays the corresponding XAS spectra and the dichroic signals. The experimental spectra are given by circles and squares for **$CrMn_3$** and MnStar, respectively. The Mn^{2+} CTM calculations have been taken from Khanra et al.[29] In contrast to these calculations, it was not possible to reproduce the Mn L-edge XAS spectra of **$CrMn_3$** assuming neither O_h nor even the C_{4h} symmetry. A highly distorted 6-fold $OClN_4$ coordination of the Mn^{II} ions leads to a strongly anisotropic exchange field, and the **$CrMn_3$** CTM calculations become challenging. In the lower panel of Figure 8, we compare the sum (XAS) over the two helicities shown in the top panel and the dichroic (MCD) signals of **$CrMn_3$** (circles) and MnStar (squares).

The characteristic two Mn L edges visible at about 640 and 652 eV originate from the spin−orbit coupling of the 2p shell representing the $2p_{3/2}$ and $2p_{1/2}$ to 3d transitions. In detail, the Mn $L_{3,2}$ XAS comprises six main features: a shoulder at approximately 639.0 eV, the Mn L_3 main peak at 640.0 eV, two additional L_3 shoulders at higher energies of 641.0 and 643.5 eV, and two peaks at the L_2 edge at 650.0 and 652.5 eV. This sequence holds for both the **$CrMn_3$** and MnStar XAS spectra, clearly revealing the Mn^{2+} ($3d^5$) valence state by force of the fact that the XAS is sensitive to the local electronic structure and chemical environment.

(47) We invite the reader to study our animations on http://spin.fh-bielefeld.de (accessed Jan 2010).

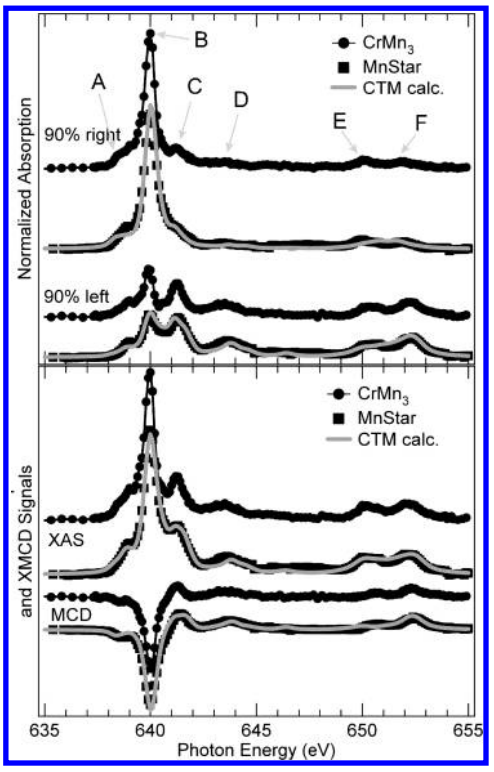

Figure 7. Dichroic Mn $L_{2,3}$ spectra of **$CrMn_3$** (circles) and the MnStar (squares) taken at a temperature of 5 K and an applied magnetic field of 5 T (top panel) and corresponding XAS and MCD signals (bottom panel). The solid lines represent the appropriate Mn^{2+}Star CTM calculations.

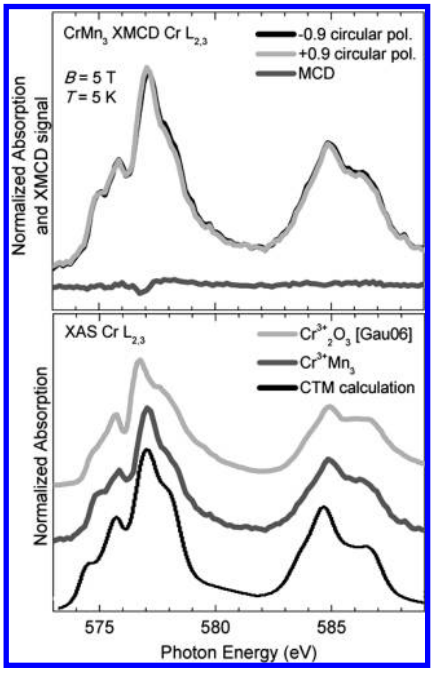

Figure 8. Dichroic Cr $L_{2,3}$ spectra and MCD signal of **$CrMn_3$** taken at a temperature of 5 K and an applied magnetic field of 5 T (top viewgraph). Comparison of the **$CrMn_3$** and Cr_2O_3,[49] Cr L edge XA spectra plotted along with CTM calculations for a Cr^{3+} ion in O_h symmetry ($10Dq = 2.2$ eV; bottom viewgraph).

To better understand the ionic Mn^{2+} behavior, it is necessary to mention that we extracted a 93.8% $3d^5$ and a 6.2% $3d^6\underline{L}$ configuration from the MnStar CTM calculations.[29] This is noteworthy, because charge transfer can result in a deformation of the multiplet structure and an appearance of satellite structures.[48] Furthermore, the local crystal-field strength around the absorbing manganese atom can be probed directly by XAS. The close resemblance of the **$CrMn_3$** and MnStar Mn XAS spectra suggests that the crystal-field splitting in **$CrMn_3$** is equally as large as in MnStar, namely, 10 Dq = 0.6 eV. Compared to values found for manganese oxides, this magnitude is rather low. However, for similar molecules like Mn_4 or $CrMn_6$, similar values of 10 Dq have been found.[29]

The upper panel of Figure 8 presents the dichroic XAS and MCD spectra of the chromium ion in the magnetic core of **$CrMn_3$** at 5 T and 5 K. Compared to the Mn^{2+} X-ray absorption spectra, the Cr^{3+} ones comprise rather broad peaks. Two main peaks are located at 577.0 and 585.0 eV for the L_3 and L_2 edges, respectively. Clear multiplet structures around the main peaks are visible. The spectrum allows to identify eight features, which are unique signatures for the Cr^{3+} ion being in an octahedral environment.[49] Looking at the XMCD signal of chromium is at first glance astonishing: no significant signal was recorded.

To get a deeper insight into the local symmetry and multiplet structure of the Cr ion, we also performed ligand-field (LF) multiplet calculations (using the TTmultiplet program) for trivalent chromium in the O_h symmetry. The result is given as the black solid line in the lower panel of Figure 8 together with the corresponding XAS Cr $L_{2,3}$ edge of Cr_2O_3 (see ref 49) and the isotropic XAS of **$CrMn_3$**. All spectra have a very similar shape. The **$CrMn_3$** XAS spectrum (dark gray) agrees nearly perfectly with the Cr_2O_3 spectrum (light gray). There is one particular feature shifting: the main peak of the Cr L_3 edge of **$CrMn_3$** is located at 577.0 eV photon energy, compared to 576.6 eV in the XAS spectrum of Cr_2O_3. Also, the relative intensities of the peaks at the L_3 and L_2 edges differ slightly. With the charge transfer multiplet calculation, we were able to reproduce the characteristic features of the **$CrMn_3$** absorption spectrum, and we find a 75.2% $3d^3$ and 24.8% $3d^4\underline{L}$ configuration.

We applied the XMCD sum rules developed by Thole and Carra, that later were confirmed experimentally by Chen et al.[30,50,51] in order to extract the element selective spin and orbital moments of the Mn^{2+} and Cr^{3+} ions in **$CrMn_3$**. From our experimental data recorded at 5.0 K, we extracted a local manganese spin moment of m_{Spin} = 7.24 μ_B per molecule (2.41 μ_B per manganese atom) and an orbital moment of m_{Orb} = 1.56 μ_B per molecule (0.52 μ_B per manganese atom).

Sum rule analysis of the experiment performed at 20.0 K yielded m_{Spin} = 3.88 μ_B and m_{Orb} = 0.015 μ_B per molecule. Because the sum rules can only be applied properly when the separation of the $2p_{3/2}$ and $2p_{1/2}$ levels is large enough to clearly distinguish the $j_{3/2}$ and $j_{1/2}$ excitations, a spin-correction factor of 1/0.680 is necessary if the spectral features of the L_2 and L_3 edges do overlap. In this case, a quantum-mechanical superposition of the $j_{3/2}$ and $j_{1/2}$ excitations appears during the absorption process. In our earlier work, we already discussed and validated this correction factor, which was first proposed and calculated by Teramura et al.[29,52,53] Using this spin-correction factor, we obtain a local manganese spin moment of m_{Spin} = 10.65 μ_B per molecule and a rather large orbital moment of m_{Orb} = 1.56 μ_B per molecule at 5 T and 5 K, whereas at a temperature of 20 K we obtain m_{Spin} = 5.71 μ_B and m_{Orb} = 0.05 μ_B. Although we find a quite good agreement between the magnetic moment obtained from the MCD and the magnetometry, we want to point out that very recently it has been found that the correction factor depends on the crystal field strength, also the nonzero orbital moment can influence the spin sum rule correction factor.[54]

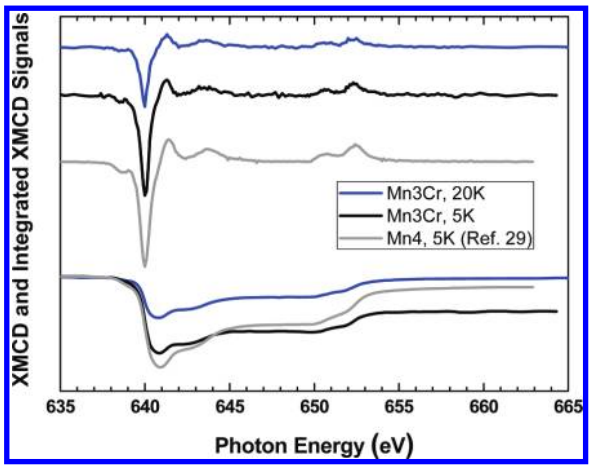

Figure 9. Experimental Mn $L_{2,3}$ MCD signals of **$CrMn_3$** recorded at 5 K (black) and 20 K (blue) and MnStar[29] (gray) plotted along with the corresponding MCD integrated intensities.

Next, we compare the above-mentioned results with those obtained on the **Mn_4** (MnStar).[29] Although the manganese $L_{2,3}$ edge MCD signals of MnStar and **$CrMn_3$** look very similar at first glance, the orbital angular-momentum distribution for these two compounds is very different. Figure 9 shows a comparison of the **$CrMn_3$** and MnStar manganese $L_{2,3}$ edge MCD signals and their integrated intensities at 5 K. The integrated intensity of the overall MCD (L_2 and L_3 edges) indicates the presence of an unquenched orbital angular Mn momentum in **$CrMn_3$** at 5 K. In contrast, for the MnStar, an almost completely quenched orbital moment is found at 5 K.[29] The result for **$CrMn_3$** is surprising because it is inconsistent with a half filled $3d^5$ state, where all d orbitals are perfectly balanced within the $\pm m$ contributions. On the one side, potential errors in the sum rule analysis, such as offset corrections or a too short integration range,

(48) van der Laan, G.; Kirkman, I. W. *J. Phys. Condens. Mater.* **1992**, *4*, 4189.
(49) Gaudry, E.; Sainctavit, P.; Juillot, F.; Bondioli, F.; Ohresser, P.; Letard, I. *Phys. Chem. Miner.* **2006**, *32*, 710.
(50) Thole, B. T.; Carra, P.; Sette, F.; van der Laan, G. *Phys. Rev. Lett.* **1992**, *68*, 1943.
(51) Carra, P.; Thole, B. T.; Altarelli, M.; Wang, X. D. *Phys. Rev. Lett.* **1993**, *70*, 694.
(52) de Groot, F.; Kotani, A. *Core Level Spectroscopy of Solid*; Taylor & Francis: London, 2008.
(53) Termamura, Y.; Tanaka, A.; Jo, T. *J. Phys. Soc. Jpn.* **1996**, *65*, 1053.
(54) Piamonteze, C.; Miedema, P.; de Groot, F. M. F. *Phys. Rev. B* **2009**, 184410.

can cause the overestimation of orbital momentums.[55a] However, we want note that the Mn ions in **$CrMn_3$** are in a strongly distorted and inhomogenous crystal field, which may lift the electronic degeneracy. A similar effect has been very recently reported for ε-Fe_2O_3.[55b] In contrast, we do not find a significant Mn orbital momentum at the temperature of 20 K (external field still 5 T). Furthermore, high-field EPR measurements performed at 10 K on **$CrMn_3$** yielded a *g* factor of 2.05 for the Mn ions.[26] That also indicates a positive Mn orbital angular momentum. One can speculate about reasons for this surprising result. It might be due to changes in the local Mn electronic structure, e.g., the Mn−ligand bond length as a consequence of structural changes taking place between 5 and 20 K. Such an effect has been observed in ε-Fe_2O_3 very recently;[55b] however, more experimental studies on the electronic and structural properties on the **$CrMn_3$** compound in this temperature range are necessary to draw any conclusion about this result.

An appropriate determination of the local chromium moment is not possible. In order to employ the spin-correction factor, a sufficiently large L_3/L_2 splitting is required to avoid problems due to the L_3-L_2 mixing.[53] In the case of chromium, this is not the case. Qualitatively, one can assume a very small local magnetic spin moment of chromium, ordered ferromagnetically with respect to the manganese spins, in **$CrMn_3$**.

Comparing the magnetization data at 5 T and 4.2 K—especially the local chromium magnetization extracted by use of the anisotropic Heisenberg model calculations (Figure 3)—with the local magnetic moments of manganese and chromium obtained from our XMCD experiments at 5 T and 5 K, we find perfect agreement. The total magnetization is about 12.5 μ_B per molecule, whereas the local chromium magnetic moment does almost completely disappear but remains ferromagnetically ordered with respect to the manganese spins (Figure 3). Also, the large local anisotropy parameter for manganese ($d_{Mn} = -1.05$ cm^{-1}) obtained from our Heisenberg simulations can be understood qualitatively. The XMCD measurements give direct experimental evidence that the orbital moments of the manganese ions are only partially quenched. *These results can be regarded as a first example of strong anisotropy and frustration effects probed by X-ray magnetic circular dichroism.*

4.3. Electronic-Structure Calculations. For density-functional calculations, the molecule was prepared in different magnetic configurations, referred to in the following according to how the spin moments of individual atoms (Cr, Mn, Mn, Mn) are set in the U (up) or D (down) direction with respect to the global quantization axis. The total energies of such configurations were compared. We calculated as well the energies for some noncollinear spin configurations but did not reach conclusive results due to convergence problems. Restricting our discussion to collinear cases only, we can emphasize the following:

1. The individual spins on the Cr and Mn positions tend to remain quite stable at values of 3/2 and 5/2, respectively, but can be inverted at relatively low energy cost.
2. The saturation value of the total spin, 18/2 as in the UUUU configuration, agrees with the results of the magnetization measurements.
3. At variance with what could have been expected, i.e., a preferential antiparallel coupling between Cr and Mn, the DUUU configuration is energetically, by 39 meV, higher compared to the UUUU configuration. However, the inversion of two spins, such as in the DDUU and other degenerate configurations, is by merely 13 meV higher in energy than the fully magnetized situation. Hence, it can be expected that a mixture of several such "two spins up, two spins down" configurations might ultimately emerge as the ground state. Apparently, this is a manifestation of strong frustration, as also evidenced by Heisenberg and classical spin dynamic simulations done in our work.
4. Obviously (for reasons typical for DFT calculations in molecular magnets where the intra-atomic correlation effects are underestimated, see, e.g., ref 56), the magnetic splitting within the 3d shells of Cr and Mn comes out too small, and consequently the HOMO−LUMO gap is strongly underestimated. However, it does not fully disappear, at least in the most "competitive" spin configurations, amounting to 0.51 eV in UUUU, 0.63 eV in DUUU, and 0.70 eV in DDUU. The latter supports the above argument that the mixing of several DDUU-like states might result in a stable and energetically favorable (frustrated) configuration.

For discussing the spatial distribution of spin density, we use the DUUU configuration, because it shows a reasonable "spin contrast" in the Cr−Mn coupling (see Figure 10).

It should be noted that each individual spin is not fully localized on a 3d center, so that the coresponding magnetic density somehow spills onto the neighboring atoms. However, the spins remain quite "rigid", in the sense that, in a different spin configuration, the spatial spin density around a given center in first approximation would be inverted (i.e., spin up becomes spin down).

The on-site magnetic spin density is quite spherical around the Mn atoms, with their half-filled and hence symmetric d shells, and pronouncedly "cube-like" at the Cr site, where in a simplified view "only" the t_{2g} orbitals are occupied. This different shape is even more pronounced in higher spin-density isosurfaces (not shown) which are more closely confined to the atom cores.

Observing the spin density spilled onto the neighbors of a 3d center, we find it octahedrally symmetric, according to the placement of oxygen atoms around the Cr site, whereas that of the Mn atoms is strongly anisotropic (Figure 10). For one thing, the Mn's are already structurally placed in low-symmetry positions; moreover, one

(55) (a) Goering, E.; Lafkioti, F; Gold, S. *Phys. Rev. Lett.* **2006**, *96*, 039701. (b) Tseng, J.-C.; Souza-Neto, N. M.; Haskel, D.; Gich, M.; Frontera, C.; Roig, A.; van Veenendaal, M.; Nogués, J. *Phys. Rev. B* **2009**, *79*, 094404.

(56) Postnikov, A. V.; Kortus, J.; Pederson, M. R. *Phys. Stat. Sol. B* **2006**, *243*(11), 2533–2572.

(57) Kokalj, A. *J. Mol. Graphics Modell.* **1999**, *17*, 176. The code is available from http://www.xcrysden.org (accessed Jan 2010).

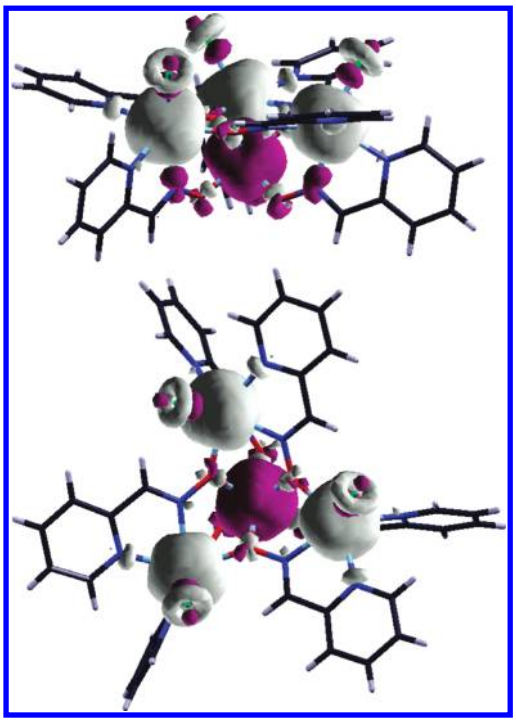

Figure 10. Two views of the spin-density isosurfaces, corresponding to $\pm 0.0025\ e/\text{Å}^3$, in the DUUU configuration of **$CrMn_3$**. Positive/negative values are indicated by light gray/dark violet color. The molecular structure is shown as a framework, with orientation and color code as in Figure 1.

can see that the Cl 3p shell, although almost fully occupied, exhibits an interesting break of symmetry in its related spin (Figure 10). This might be an important source of anisotropy found for the Cr atoms in the spin-Hamiltonian simulations, as was already mentioned in section 4.1.

5. Conclusions

In summary, we presented a comprehensive investigation of the electronic structure and the magnetic properties of the star-shaped heteronuclear $Cr^{III}Mn^{II}_3$ complex. Various X-ray spectroscopic methods were used to investigate the internal chemical, electronic, and magnetic structure of **$CrMn_3$**. The XAS spectra of the manganese and chromium L edges were measured and compared to Mn^{2+} Star spectra investigated earlier[29] or modeled within the ligand-field multiplet model, respectively, in order to investigate the valence and local symmetry. Crystal-field and charge-transfer parameters were extracted from the calculations and are in good agreement with earlier data.

Using magnetization measurements, element-selective XMCD at the Mn and Cr L edges, and quantum model calculations based on an anisotropic Heisenberg Hamiltonian, we were able to understand the complete magnetic structure of the **$CrMn_3$** magnetic core, including the manganese single-ion anisotropy and frustration. The experimental data fit perfectly to the quantum calculations, allowing an accurate determination of the exchange interactions and of the dominant local anisotropies. The extracted parameters were used to perform classical spin-dynamic simulations. The field-dependent classical ground state and low-temperature properties were studied in our extensive work on the **$CrMn_3$** complex.

Acknowledgment. E. Arenholz and J. D. Denlinger are acknowledged for excellent technical support. We would like to thank Joris van Slageren for discussing anisotropy issues with us and for drawing our attention to recent publications on Mn(II) anisotropies. Financial support by the Graduate College and the PhD program (Lower Saxony) is gratefully acknowledged. A.V.P. acknowledges the use of computing resources of the PMMS of the Paul Verlaine University. Part of the work was performed at the Advanced Light Source (A.L.S.), which is supported by the U.S. Department of Energy under Contract No. DE-AC03-76SF00098.

Financial support from the German Research Council (DFG) in the priority program "Molecular Magnetism" as well as through the research group FOR 945 is also thankfully acknowledged.